

# 2

---

## The STARE instrument

In this chapter we describe the STARE (STellar Astrophysics and Research on Exoplanets) project, which involves the STARE instrument (a  $\sim 10$  cm wide field Schmidt camera) and its data analysis (based on Differential Imaging techniques), needed to identify the transiting planet candidates.

### 2.1 Introduction: The STARE instrument

THE telescope is a field-flattened Schmidt design (Figures 2.1 and 2.2), with an aperture of 102 mm and a effective focal length of 296 mm, giving an  $f$  ratio of 2.9. To make the focal plane accessible, it has a diagonal mirror that is mounted to the aluminum tube assembly with a delrin spacer. The length of this spacer is chosen to compensate temperature-induced focus drifts. After the diagonal mirror and near the focal plane there is a system of three manually changeable filters. These were chosen to resemble the Johnson's standard filters B, V and R. Due to the poor sensitivity of the CCD detector to the blue wavelengths, the filter response of the B and V filters were shifted to the red. Thus, the absolute photometric calibrations would require special care. For our purposes, though, time series will be obtained in the R filter, and B and V color images of the stars are taken once per field (typically on a clear moon-less photometric night, with the field close to the zenith), to estimate the spectral types of the stars. Our interest will reside in the relative magnitudes of the stars obtained in the R filter; thus, these shortcomings in the absolute calibrations are of little importance.

The wave front coming out from the filter slide is not flat, and it needs to

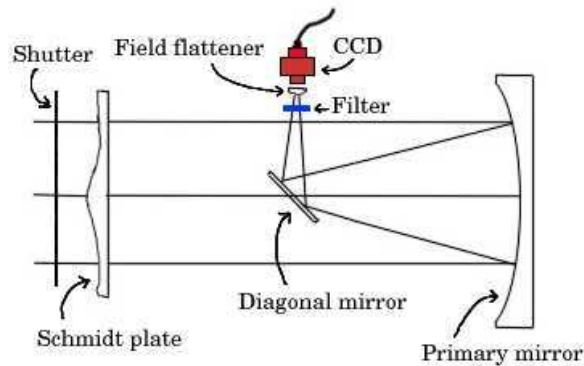


FIGURE 2.1— Optical scheme of the STARE telescope.

be flattened before it arrives to the CCD detector. This is achieved by a plano-convex lens that is oiled to the front surface of the dewar's window. In order to minimize the distance between the detector and the diagonal mirror, we placed the shutter in the entrance pupil. This is achievable thanks to the small diameter of the mirror. The main drawback of this action is that the shutter takes a non-negligible time to open and close ( $\sim 0.4$  s, with several tenths of a second between the center and the corners of the frame), and this difference in exposure times needs to be taken into account in the data reduction scheme.

The CCD detector is a 2Kx2K front-illuminated Loral device installed in a camera fabricated by Pixel Vision Inc. The square pixels are 15-microns wide. It is cooled down to  $-35^\circ$  C with a 3-stage thermoelectric cooler. The readout time is 13s at a speed of 400kHz; at this rate, the read noise is 10 electrons. We operate the system with a gain of 6.8 electrons per analog-to-digital converter unit (ADU).

The dark current of the camera at its operation temperature is  $\sim 0.8$ - $0.9$  photoelectrons per pixel per second. To avoid negative counts, it has an additional signal (bias) that is typically 200 ADU's. This signal can be measured with null-time exposures or with a region of the CCD that is never exposed to light (the overscan region).

The sky signal at its current emplacement on the Observatorio del Teide of the Instituto de Astrofísica de Canarias, for a moon-less sky is always above 400 counts in a typical 107 s exposure. Thus, the dark and readout noises are always lower than the sky background photon noise ( $\sqrt{400} = 20$  counts).

With this optical assembly, the total field of view covered in the sky is

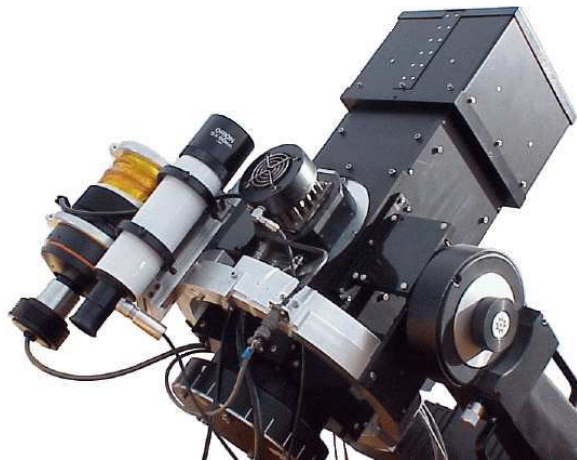


FIGURE 2.2— The STARE telescope.

$6.1 \times 6.1 \text{ deg}^2$ . The image scale is then 10.8 arcsec per pixel.

### 2.1.1 The mount

All the above components of the telescope are attached to a commercial Meade LX-200 fork mount (made for a 12-inch telescope). This mount allows continuous following of a field from dusk to dawn. But it is not precise enough as to maintain all the stars within the same 1 - 2 pixels all night. To accomplish this, the telescope has a 90 mm Maksutov reflector piggy-backed, equipped with a Santa Barbara Instrument Group ST-4 autoguider. This system takes images of a bright ( $\sim 5$  mag) star every 2 s, and corrects the mount drifts to guide on the star. There is flexure between the main telescope and the guiding system during a night that needs to be compensated. To achieve this, every science image taken with the main CCD is compared to a couple of  $128 \times 128$  sub-images of the field<sup>1</sup>, and corrections to the position of the star in the ST-4 camera are done if necessary. This comparisons are performed at the same cadence as the science data is arriving, which is typically once every two minutes.

The telescope and mount are inside a 3.2 m diameter Ash-Dome, which needs to be manually opened, and it is connected to the *Cielo Nocturno* building

<sup>1</sup>One image is the central part of a reference image taken at the beginning of the campaign. The second image is the central  $512 \times 512$  pixels of the same reference image, re-sampled to  $128 \times 128$  pixels.

with optical fiber. Several views of the instrumentation are given in Figures 2.3 and 2.4.

### 2.1.2 The computers

The UPS (Uninterrupted Power Supply), computers and data storage devices are inside the *Cielo Nocturno* building. Two linked Pentium PC computers operate the whole system: Butch and Sundance. Butch is responsible for the dome and mount control, while Sundance controls the CCD acquisition and storage. The communication between Sundance and the CCD is done with a dual optical fiber serial line. Both computers operate under Windows 98, and the user interface consists of several programs written in Visual C++. These invoke scripts which are based on “Orchestrate Scripting Software” for the telescope control, and “AutomaDome” for the dome control; both are by Software Bisque. STARE’s operation is not fully autonomous, however. It depends on an operator who decides to start the system if observing conditions are acceptable. The operator has to remove the telescope covers, open the dome manually, and start a telescope control script. This script will begin the observations at a specified hour, once a sample field reaches a prescribed altitude or when the sky is dark enough. The telescope will then perform the entire observing programme autonomously. At the end of a night, or once a sample field moves too low, the telescope parks itself in a safe position (no direct sunlight on the telescope), and waits for the return of the operator. He/she will then close the dome and create copies of the acquired data. The operator is also required to monitor meteorological conditions and has to shut down the instrument in case of adverse conditions. These tasks are performed by operators who are responsible for several instruments at Teide Observatory, avoiding the need for dedicated manpower.

## 2.2 Data Analysis

The state-of-the-art concept to perform photometry on crowded CCD images is the Differential Imaging Analysis (Alard & Lupton 1998, Alard 2000). Basically, it consists of choosing one high quality image of the field, taken at the best possible conditions of seeing and atmospheric transparency. We will refer to this image as the reference image. Every science image is shifted, interpolated to the same grid as the reference frame and convoluted with a kernel image, in order to correct for possible seeing and focus variations, and then subtracted from the reference image. The photometry is later done on the resultant image, which should only have significant signal in the objects whose flux has changed from the reference image. These include variable stars, asteroids, artificial



FIGURE 2.3— Different views of the STARE instrument. From top left to bottom right: dome, telescope shutter, out-of-limits sensor, control computers, mount keypad, telescope electronics rack.

satellites and trailing stars, among others. In this section, we describe in more detail all the process, from the calibrated images and the standard star list to the final light curves.

### 2.2.1 Calibrating the images

All the science images are corrected for the usual effects needed to perform CCD photometry, namely:

- Bias subtraction. 20 images with the shortest exposure time allowed by the software (1s) and the telescope covered are a relatively good measurement of the ideal 0s exposure time image. They are taken every observing night, and averaged (and sigma-clipped) to produce one master bias image for that night. This image is zero-scaled with the overscan region of every science image taken on that night, and subtracted from it.



FIGURE 2.4— Different views of the STARE dome. From top left to bottom right: emergency stop button, dome control panel, flat-field lamp, flat-field screen.

- Flat field correction. The differences in the response of the different CCD pixels, and the effect of the vignetting affecting the telescope are corrected with a division of every science image by an image of an uniformly illuminated field. These images are taken following two approaches: images taken at twilight, and images taken pointing to a screen located at the dome, which is illuminated by a lamp. The twilight images provide a measurement of the large-scale structures, but it is difficult to accumulate enough photons to measure the small-scale gain structure accurately. This is achieved with the dome images, in which more photons can be accumulated, but it is hard to achieve a constant illumination throughout the field of view. Thus, a combined flat-field is constructed using the sky-twilight images as a measurement of the large-scale structures, while the small-scale structures are measured with the dome flats. Typically, one master flat field, constructed using a combination of all the available

flat images in the observing period of one specific campaign, is used to correct all the images of the campaign.

- Dark current correction. The non-zero temperature operation of the CCD causes several ADUs to arise from thermal action. The signal depends on the temperature of the CCD and on the pixel impurities. This signal can be measured taking long exposures with the telescope covered (the electrons due to dark current accumulate at a constant rate for each pixel). All the signal appearing in these images is the bias + the effect of the temperature. Typically, 20 images of 600 s exposure time are taken in cloudy nights, and averaged to get a master dark image that is scaled to the science images exposure time before being subtracted.
- Shutter correction. The non-negligible open-close time of the shutter located at the entrance of the telescope makes the final exposure time of the science images be bigger at the center of the images than at the corners. Dome flat field images taken with the same illumination and with different exposure times are used to build an artificial image that will contain the shutter open+close time at every pixel.

Nine 128x128 subimages of a reference image (ref1) are chosen to estimate the translation, rotation and scale changes on a nightly basis. The position of one reasonably isolated star in the field is used to get a first rough measurement of the sky background level and the atmospheric transmission. Quality-control plots are computed and stored for each observing night; an example of these plots for one typical night is presented in Figure 2.5. These plots are used to better filter the data, eliminating from the further analysis the images with doubtful quality due to weather or technical problems.

### 2.2.2 Building a star list

After a visual inspection of the quality-control plots, one image with one of the lowest sky background levels is chosen to construct a star list of all the objects whose light curves are desired. This image (ref2 hereafter) is inspected for unusual signals, such as satellite or plane trails, meteors, diffuse light, etc. Using DAOPHOT/ALLSTAR (Stetson 1987, Stetson & Harris 1988, Stetson 1992), a star list containing the PSF magnitudes of several tens of thousands of stars is built (typically, from  $\sim 8000$  stars until  $\sim 40000$ , depending on the stellar crowding). A few dozen stars distributed through all the field of view are identified with the Tycho-2 catalogue<sup>2</sup>, and the transformation between the

---

<sup>2</sup>Available at [http://www.astro.estec.esa.nl/hipparcos\\_scripts/hipMultiSearch.pl](http://www.astro.estec.esa.nl/hipparcos_scripts/hipMultiSearch.pl)

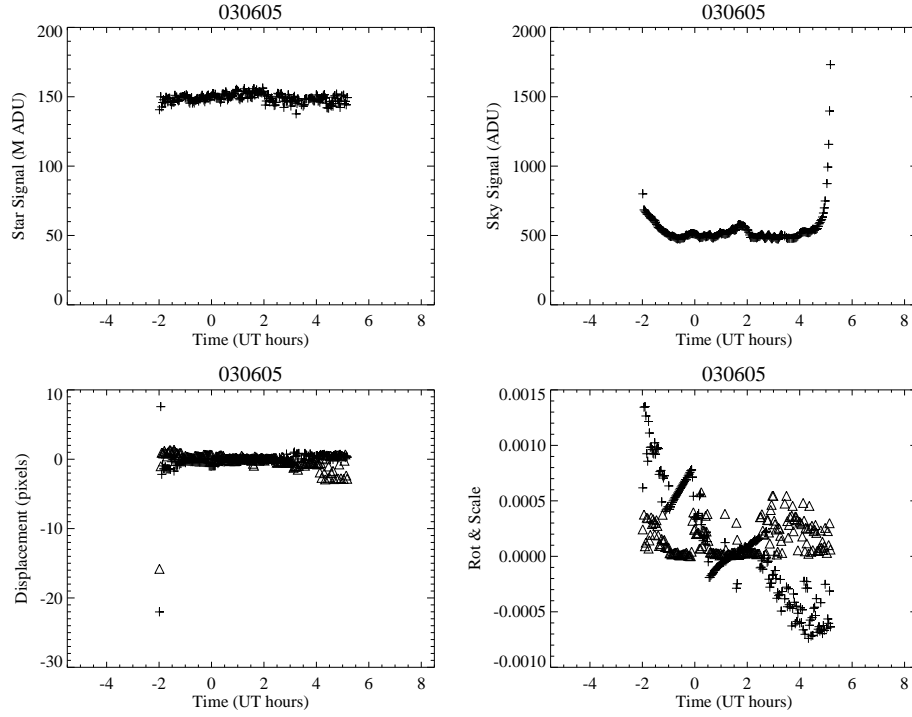


FIGURE 2.5— Plot for quality evaluation in a good night of observation. Top left: The signal of a bright unsaturated star. Top right: The sky signal. Bottom left: The displacement of the image from the ref1 image. Bottom right: The field rotation and scaling trends during the night.

CCD's X and Y coordinates and J2000.0 Right Ascension and Declination is extrapolated for the rest of the stars in the star list.

### 2.2.3 Interpolation to the same X-Y grid

Before performing the image subtraction, all the images have to be interpolated to the same X-Y grid as the ref2 image. This is done with the routine *interp.csh* of the ISIS package, which requires as input parameters the coefficients for the transformation. These are calculated by the least square solution to the relations:

$$x = a_0 + a_1 y_{ref2} + a_2 x_{ref2} + a_3 y_{ref2}^2 + a_4 x_{ref2} y_{ref2} + a_5 x_{ref2}^2 \quad (2.1)$$

$$y = b_0 + b_1 y_{ref2} + b_2 x_{ref2} + b_3 y_{ref2}^2 + b_4 x_{ref2} y_{ref2} + b_5 x_{ref2}^2 \quad (2.2)$$

where the  $x$  and  $y$  coordinates are from the image to be interpolated, and  $x_{ref2}$  and  $y_{ref2}$  are those of the ref2 image. The  $x$  and  $y$  coordinates for each star in the star list and in each data image are calculated with aperture photometry (APHOT), and matched to the same stars with  $x_{ref2}$  and  $y_{ref2}$  coordinates in the ref2 image with DAOMATCH/DAOMASTER (Stetson 1993).

### 2.2.4 Image subtraction

A higher S/N image (hereafter ref3) is built from a set of typically 10-20 images taken the same night and at similar times as the ref2 image. All these images have to be interpolated, and they are combined with the routine *ref.csh* of the ISIS package. The ref3 image is then convolved with an optimal kernel  $K$  to match each data image's psf profile, and the data image is subtracted from this ref3 image. The kernel  $K$  is computed by a least square minimization of the expression (Alard 2000):

$$\sum_i ([R \otimes K](x_i, y_i) - I(x_i, y_i))^2 \quad (2.3)$$

in which the kernel is assumed to be well decomposed in the basis functions:

$$K(u, v) = \sum_n a_n K_n(u, v) \quad (2.4)$$

with:

$$K_n(u, v) = e^{-(u^2+v^2)/2\sigma_k^2} u^i v^j \quad (2.5)$$

and the generalized index  $n = (i, j, k)$ .

The resulting image will have only significant signal in the variable and moving objects (Figure 2.6). As a consequence of the undersampling of the STARE's PSF, there will also be some residuals in the positions of the bright stars.

After image subtraction on a typical field of a STARE campaign, there are several thousand of residual images that are in the same x-y grid. It is thus straightforward to perform aperture photometry to measure the residuals centered on the positions of the stars in the star list. Let's write the residual flux of a star  $s$  in the  $i$ th image as  $\Delta F_{s,i}$ , with its associated standard error of  $\sigma_{\Delta F_{s,i}}$ . This set of images will include the ref3 image subtracted from itself. We will write the flux of the star  $s$  in this subtracted image as  $\Delta F_{s,R}$ . The flux of the star in the ref3 image is, to a good approximation, the measured flux in the ref2 image, used to build the star list. We will refer to this flux as  $F_{s,R}$ .

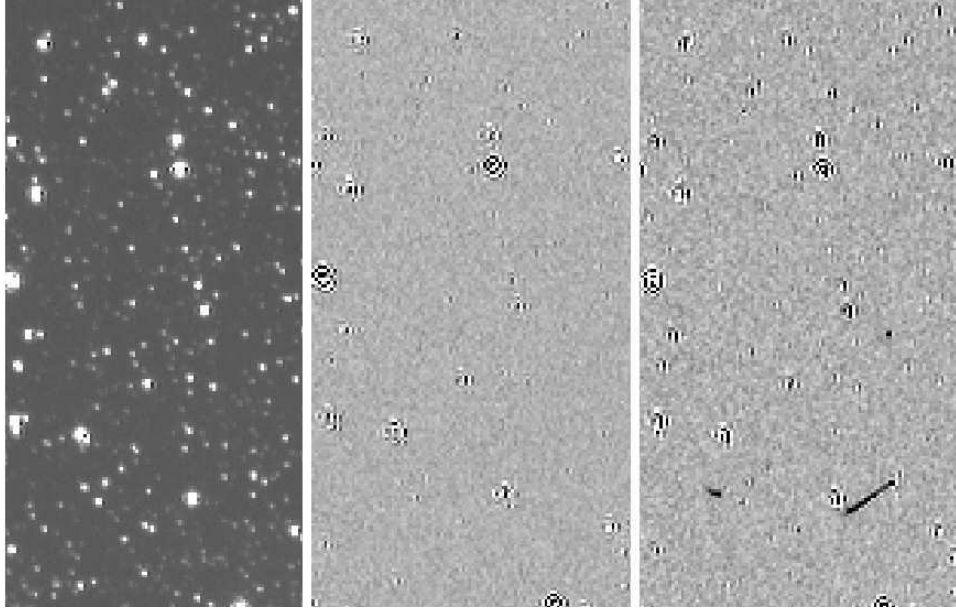


FIGURE 2.6— Left: A  $100 \times 200$  pixels subimage of the ref2 image. Center: The same part of the image for the subtracted ref2 image. Right: The same part, for another image of the campaign, with worse weather conditions. The diagonal line is consequence of a falling star (present in the image  $i$ , but not in the ref2 image).

Then, the magnitude difference of the star  $s$  in the  $i$ th frame with respect to its magnitude in the ref3 image is obtained by:

$$\Delta m_{s,i} = -2.5 \log \left( \frac{F_{s,0} - \Delta F_{s,i}}{F_{s,0}} \right) \quad (2.6)$$

where  $F_{s,0} = F_{s,R} + \Delta F_{s,R}$  is the flux of the star in the ref3 image. The associated error can be estimated from the error in the ref3 image:  $\sigma_{\Delta m_{s,i}} = 1.0857(\sigma_{F_{s,i}}/F_{s,0})$ , where  $\sigma_{F_{s,i}}^2 = \sigma_{F_{s,0}}^2 + \sigma_{\Delta F_{s,i}}^2$ .

The resulting photometry is reformatted and collected in files which contain a manageable number of stars (typically 2000) with all the measurements for those stars, ordered in HJD.

These light curves are highly correlated, showing systematic trends that could not be removed in any of the previous steps. To correct for these trends, each star's light curve is regressed with the rest of the stars. This is done by a general linear least squares solution using Singular Value Decomposition (SVD) techniques (see, for instance, Press et al. 1988). In our case, each star's light

curve ( $m_s = m_{s,0}, m_{s,1}, \dots, m_{s,M-1}$ , with  $M$  the total number of observations) can be expressed as:

$$\begin{pmatrix} m_{s,0} \\ m_{s,1} \\ \vdots \end{pmatrix} = \begin{pmatrix} m_{0,0} & m_{1,0} & \dots \\ m_{0,1} & m_{1,1} & \dots \\ \vdots & \vdots & \ddots \end{pmatrix} \cdot \begin{pmatrix} x_0 \\ x_1 \\ \vdots \end{pmatrix} \quad (2.7)$$

The solution vector  $\mathbf{x} = x_0, x_1, \dots, x_{N-1}$  (with  $N$  the total number of stars), for non-square matrices, is calculated as the vector that minimizes the expression:

$$\chi^2 = |\mathbf{A} \cdot \mathbf{x} - \mathbf{b}|^2 \quad (2.8)$$

where  $\mathbf{A}$  is the first matrix in the righthand side of the Equation 2.7 and  $\mathbf{b}$  is the term on the lefthand side, i.e., the magnitudes of the star  $s$ . The solution of the least-squares problem can be written as:

$$\mathbf{x} = \sum_{i=0}^{M-1} \left( \frac{\mathbf{U}_{(i)} \cdot \mathbf{b}}{w_i} \right) \mathbf{V}_{(i)} \quad (2.9)$$

where  $\mathbf{U}$  is an column-orthogonal  $M \times N$  matrix,  $\mathbf{V}$  is a  $N \times N$  orthogonal square matrix, and  $w_i$  are the *singular values*, or the elements in the diagonal of a  $N \times N$  diagonal  $\mathbf{W}$  matrix that satisfy:

$$\begin{pmatrix} \mathbf{A} \end{pmatrix} = \begin{pmatrix} \mathbf{U} \end{pmatrix} \cdot \begin{pmatrix} w_0 & & & \\ & w_1 & & \\ & & \dots & \\ & & & w_{N-1} \end{pmatrix} \cdot \begin{pmatrix} \mathbf{V}^T \end{pmatrix} \quad (2.10)$$

The variance in the parameter  $x_j$  is:

$$\sigma^2(x_j) = \sum_{i=0}^{M-1} \left( \frac{V_{ji}}{w_i} \right)^2 \quad (2.11)$$

The final light curves will have part of this least square solution subtracted, i.e.:

$$\mathbf{m}'_s = \mathbf{m}_s - \mathbf{A}' \cdot \mathbf{x} \quad (2.12)$$

where the matrix  $\mathbf{A}'$  is an approximation of the matrix  $\mathbf{A}$ , built with only the largest singular values  $w_i$ . We obtain good results in a typical field of STARE by de-correlating no more than 500 stars at once, because this method

requires more data points than stars. The final light curves of real variable stars remain basically unaffected, while the variations that are common to the majority of the stars are mostly removed with this method. We noticed, though, that the amplitude of the genuine events (such as transits) are decreased by a 10-20%, which can affect to the detectability of the low depth transit events.

The last step in the light curve building is the averaging of the data into 0.0062 d ( $\sim 9$  min) wide bins (typically, 4-5 data points per bin). This reduces the final dispersion of the brightest stars from  $\sim 6$  mmags to  $\sim 3$  mmags.

### 2.2.5 Transit search

The binned light curves of all the stars are searched for transit shaped signals with the BLS algorithm (Kovács, Zacher, & Mazeh 2002). This algorithm computes the Signal Detection Efficiency (SDE), defined as:

$$SDE = \frac{SR_{peak} - \langle SR \rangle}{\sigma_{SR}} \quad (2.13)$$

where SR is the Signal Residue of the time series at any given trial period (defined below).  $SR_{peak}$  is the SR at the highest peak,  $\langle SR \rangle$  is the average, and  $\sigma_{SR}$  is the standard deviation of SR over the frequency band tested. The SR at a trial period is computed as:

$$SR = MAX \left\{ \left[ \frac{s^2(i_1, i_2)}{r(i_1, i_2)[1 - r(i_1, i_2)]} \right]^{1/2} \right\} \quad (2.14)$$

where  $i_1$  and  $i_2$  are the sorted points in the phase-folded light curve with the trial period, that define a step function (box-shaped) with the values  $L$  in  $[i_1, i_2]$ , and  $H$  in  $[1, i_1)$  and  $(i_2, n]$ , with  $n$  the total number of points. The values of  $s$  and  $r$  are given respectively by:

$$s = \sum_{i=i_1}^{i_2} w_i x_i \quad (2.15)$$

$$r = \sum_{i=i_1}^{i_2} w_i \quad (2.16)$$

with  $x_i$  the phase-sorted magnitude values, associated to a weight  $w_i$ , defined as  $w_i = \sigma_i^{-2} [\sum_{j=1}^n \sigma_j^{-2}]^{-1}$ . The  $\sigma_i$  are the measurement errors of each data point. Each light curve needs to verify that  $\mathbf{w}\mathbf{x}$  has a zero arithmetic average.

The algorithm is run in each 2000 stars file, trying periods typically in the range 1 to 10 days, with 50 phase bins and fractional transit durations in the

range [0.01, 0.1]. All the stars returning values of the SDE above typically 2.7 are visually inspected, to discard obvious false positives, such as variable stars, eclipsing binaries and stars with problematic photometry. This value of the SDE was chosen after an inspection of the SDE distribution of all the stars, retaining those that have SDE above the point in which this distribution falls to  $\sim 1/3$  of its maximum value.

### 2.3 Noise sources and performance

There are several factors that contribute to the final dispersion of the unbinned light curves. These are:

- Photon noise from the star: assuming a Poisson distribution of the photon (or shot) noise, the associated uncertainty in mags is given by:  $\sigma_{star} = 1.0857/\sqrt{N}$ , being  $N$  the total number of electrons ( $= N_{ADU} \cdot gain$ ) recorded at the detector inside the star aperture, with the sky background subtracted.
- Photon noise from the sky background: the relative uncertainty in mags is given by  $\sigma_{sky} = 1.0857 \cdot \sqrt{N_{sky} \cdot gain \cdot n_{star}}/N$ , where  $N_{sky}$  is the measured sky level around the star (typically in an annulus with inner radius of 6 pixels and an outer radius of 12), and  $n_{star}$  is the number of pixels inside the stellar aperture.
- Scintillation noise: estimated using the empirical relationship by Young (1967):

$$\sigma_{sci} = 1.0857 \cdot 0.09 \cdot D^{-2/3} \cdot (1/\cos Z)^{1.75} \cdot \exp -h/h_0/\sqrt{2 \cdot T} \quad (2.17)$$

where  $D$  is the aperture of the telescope, in cm,  $Z$  is the angle in degrees from the zenith,  $h$  is the observatory altitude, in meters,  $h_0$  is the typical altitude scale height (8000 m), and  $T$  is the exposure time, in seconds.

- Detector noise sources: the reported read noise level ( $R$ ) for the detector we use is  $10 e^-$ . We can estimate the implied uncertainty in a single measurement from Everett & Howell (2001):

$$\sigma_{read} = 1.0857 \frac{R \sqrt{n_{star}[1 + n_{star}]/n_{sky}}}{N} \quad (2.18)$$

where  $n_{sky}$  is the number of pixels used to measure the sky level (in the annulus defined above).

The dark current standard deviation will be as well:

$$\sigma_{dark} = 1.0857 \sqrt{\frac{N_{dark} \cdot T \cdot n_{star} [1 + n_{star}] / n_{sky}}{N}} \quad (2.19)$$

where  $N_{dark}$  is the number of  $e^-$  per second per pixel registered at the detector. Typical values in our case are  $0.8-0.9 \text{ e}^- \text{ s}^{-1} \text{ px}^{-1}$ .

- **Uncorrected atmospheric extinction** The wide field of view of the STARE images make it challenging to achieve good atmospheric extinction corrections throughout the whole field, specially when the observing conditions were not photometric.

In the case of a field observed by STARE (a field in the constellation of Lyra, whose reduction will be described in Chapter 4), the observed dispersion of the unbinned (2-min sampled) data together with the modelling of the main noise sources are plotted in Figures 2.7 and 2.8. In those Figures, it can be seen that the main noise sources are the sky background noise for faint stars (fainter than  $R=10.4$  in full moon conditions, and  $R=12.2$  if there is no moon), and the scintillation noise for the brightest stars (estimated at an altitude of 2400 m, and at a zenithal distance of  $50^\circ$ , which corresponds to an airmass of 1.56; the values for  $n_{star}$  and  $n_{sky}$  are 13 and 339 respectively). It seems that the bright end of the sample is still above the expected noise value, which may be due to an underestimation of the scintillation noise level, uncorrected atmospheric extinction, flux errors introduced by the interpolation of the images, a non perfect guiding of the telescope, or a combination of all these factors.

## 2.4 STARE as a part of TrES

Since spring 2003, the STARE observations are coordinated inside the TrES (**Transatlantic Exoplanet Survey**) network. This consists of two other small instruments with similar characteristics as STARE, namely PSST (Dunham 2004) and Sleuth (O'Donovan, Charbonneau, & Kotredes 2004); these characteristics are summarized in Table 2.1. The advantages of these coordinated efforts, with instruments located at different longitudes, lie in:

- Less observing time per telescope is needed to detect planets with 3-5 d periods, and thus a survey of more stellar fields, without losing detection capabilities, is possible.
- Confirmation of doubtful candidates, and isolated events, such as candidates only showing ingress-egress of a transit.

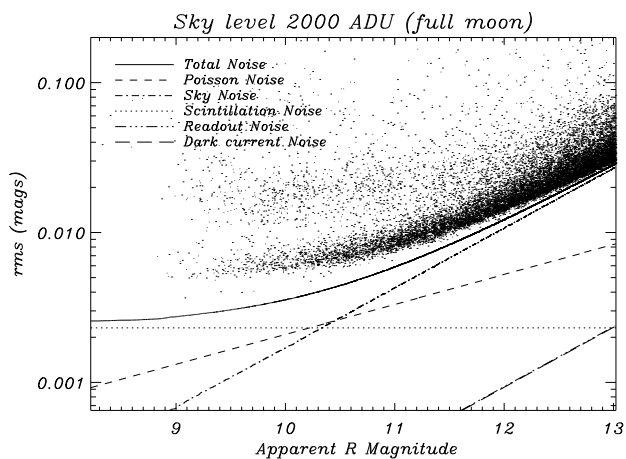


FIGURE 2.7— The unbinned decorrelated rms of all the stars in a whole STARE campaign centered on a field at the constellation Lyra (described in detail in Chapter 4). Also plotted are the main noise sources, for a typical full moon sky background. See text for details.

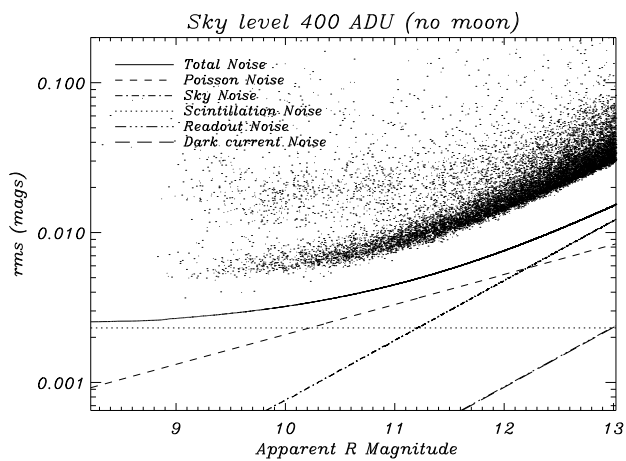


FIGURE 2.8— Same as Figure 2.7, but with the noise sources estimated for the best achievable sky background conditions at the Observatorio del Teide.

TABLE 2.1— The TrES telescopes

	STARE	PSST	Sleuth
Diameter (cm)	10.2	10.7	10
Focal Length (mm)	296	300	280
f/ ratio	2.9	2.8	2.8
Camera + pixel size	2k×2k×15 $\mu$ m	2k×2k×15 $\mu$ m	2k×2k×13.5 $\mu$ m
Camera type	front-illuminated	back-illuminated	back-illuminated
FOV	6°.1×6°.1	5°.6×5°.6	6°×6°
Mount	Meade	Celestron	Meade
Autoguider	SBIG ST-4	SBIG ST-4	SBIG ST-4
Filters	Johnson	Bessell	SDSS
Location	Tenerife (Spain)	Arizona (USA)	California (USA)
Reference	This work	Dunham 2004	O'Donovan et al. 2004

- Reduced aliasing in the spectra of the pulsating stars.
- Higher probabilities of detecting relatively long-period planets (P>10 d).